Fall 2015

Freeform extrusion fabrication of titanium fiber reinforced 13-93 bioactive glass scaffolds

Albin Thomas

Department:

FREEFORM EXTRUSION FABRICATION OF TITANIUM FIBER REINFORCED 13-93 BIOACTIVE GLASS SCAFFOLDS

by

ALBIN THOMAS

A THESIS

Presented to the Faculty of the Graduate School of the

MISSOURI UNIVERSITY OF SCIENCE AND TECHNOLOGY

In Partial Fulfillment of the Requirements for the Degree

MASTER OF SCIENCE IN MECHANICAL ENGINEERING

2015

Approved by

Ming C. Leu, Advisor
Gregory E. Hilmas
Yue-Wern Huang

ABSTRACT

Although implants made with bioactive glass have shown promising results for bone repair, their application in repairing load-bearing long bones is limited due to their poor mechanical properties as compared to human bones. This thesis study is on freeform extrusion fabrication of silicate based 13-93 bioactive glass scaffolds reinforced with titanium fibers. A composite paste was prepared with 13-93 bioactive glass filled with titanium fibers (~16 μm in diameter and aspect ratio of ~250) having 0.1 to 0.4 vol. % of the bioactive glass scaffold. This paste was then filled into a syringe manually, and then extruded through a nozzle to fabricate scaffolds with an extrudate diameter of about ~0.8 mm. The sintered scaffolds, with and without titanium fibers, had measured pore sizes ranging from 400 to 800 μm and a porosity of ~50%. Scaffolds produced with 0.4 vol. % titanium fibers were measured to have a fracture toughness of ~0.8 MPa•$m^{1/2}$ and a flexural strength of ~15 MPa .Bioactive glass scaffolds without titanium fibers had a toughness of ~0.5 MPa•$m^{1/2}$ and strength of ~10 MPa. The addition of titanium fibers increased the fracture toughness of the scaffolds by ~70% and flexural strength by ~40%. The scaffolds' biocompatibility and their degradation in mechanical properties *in vitro* were assessed by immersing the scaffolds in a simulated body fluid over a period of one to four weeks.

ACKNOWLEDGMENTS

Frankly speaking, initially academic research was a mode for me to earn financial support. This perception changed over the course of time due to some wonderful people I met and experiences that trained me. Thanks to the God for this.

For a new comer like me, doing research was something really scary. It's my advisor, Dr. Ming C. Leu who patiently guided me and made me understand that being humble and working hard is the key to being successful. The working methodology, motivation and personal values I learned from him will inspire and guide me throughout my life.

I would also like to express my deepest gratitude to Dr. Gregory E. Hilmas for the prompt advice and help he provided. His research group and lab machines made the mechanical testing part of my research an easy one.

One of the unique experiences I had in research was in cell culture and *in-vivo* studies. Being from a mechanical engineering background this part added a new level of understanding and excitement in me. Thanks to Dr. Yeu-wern Huang for his patience and guidance in this direction.

I would like to thank Krishna Kolan for the mentoring and care he provided throughout my academic life. Without his help my MS degree would have taken another two years. In addition I express my sincere thanks to Dr. Jeremy Watts, Ryan Grohsmeyer, Larry Tolliver, Eric Bohannan, Clarissa Wisner and the VRAM lab members for helping me with various research activities.

I also thank my parents and friends for the encouragement, support and attention they gave to me. I thankfully acknowledge all the sponsors for the funding they provided. Without them I would not have been able to ask for a 'MO code' very often!

TABLE OF CONTENTS

LIST OF ILLUSTRATIONS

LIST OF TABLES

1. INTRODUCTION

Bone possesses the intrinsic capacity for regeneration as part of the repair process in response to injury, as well as during skeletal development or continuous remodeling throughout adult life [1, 2]. Segmental bone defects and multiple fractures constitute a major portion of the musculoskeletal disorders seen in human beings. The current approaches towards treatment of such disorders include the use of intramedullary nailing, use of plates, and external fixations. The limitations associated with such methods include prolonged course, poor reliability, high complication rate, and poor healing rates [3]. Another sophisticated and established method of treatment of bone repairs is the use of allografts. But the lack of structural integrity, limited availability, and morbidity of the donor site pose serious limitation to this approach [4].

Over the past 10 years, biomaterials have been widely used in bone repair applications [5, 6]. A large number of synthetic substitutes like hydroxyapatite, calcium phosphate cements and glass ceramics have been investigated for bone repair [7, 8, 9, 10, 11, 12]. Even though the above materials have osteoconductive and osteoinductive properties, they provide minimal structural support. Fu *et al*.[13], Liu *et al*.[14], Kolan *et al*.[15], Doiphode *et al*[16]., and Rahaman *et al*.[17] studied the use of 13-93 bioactive glass in fabricating scaffolds for bone repair using a variety of fabrication techniques including slip casting, polymer foam replication, selective laser sintering, and robocasting. The investigation into mechanical and biological properties of the fabricated scaffolds has shown that 13-93 glass has favorable properties in repairing segmental bone defects [18, 19].

Most of the previous studies on 13-93 bioactive glass (bioglass) done by Rahaman *et al.* [18,19] have shown that the mechanical properties of 13-93 scaffolds fabricated by extrusion deposition are promising for applications in loaded bone repair. *In-vivo* assessment of 13-93 bioglass has shown good bonding between the scaffold and the surrounding tissues, in addition to new bone and tissue growth around the scaffold [20, 21, 22]. However within four weeks of implantation, cracks were generated on the surface of the scaffolds due to reaction of the bioglass with blood, resulting in the formation of hydroxyapatite [23]. These cracks could potentially cause failure of the implant. Other bioglasses with slower conversion rates could be used for implants, but at the expense of unconverted glass that will remain in the host body.

As to provide more structural integrity for the scaffolds, we propose addition of ductile metallic fibers into the bioglass matrix to form a composite with improved toughness. The addition of metallic fibers is expected to improve the ductility and lower the rate of degradation *in vivo* of the sintered scaffolds. Previous studies have shown that the strength and toughness of glasses are improved upon dispersion of metallic particles in them [24, 25, 26].

In this study, titanium fibers are used to reinforce the bioglass matrix for fabrication of scaffolds. Titanium is used due to the following reasons:1) titanium is an FDA approved, widely used material for synthetic implants as it offers excellent biocompatibility; 2) the thermal coefficients of expansion of the titanium fiber and bioactive glass are close to each other, thereby reducing the localized thermal stresses that may be generated during the

fabrication process; and 3) the presence of silica in bioglass matrix and titanium oxide on the surface of titanium fibers will essentially provide good adhesion between these materials, thereby avoiding problems like de-bonding and voids.

Several additive manufacturing techniques are used in the fabrication of bioglass scaffolds. Cesarano *et al*. [27] used robocasting technique to fabricate HA latticework structures for load bearing bone repair applications. Lorrison *et al*. [28] used selective laser sintering to fabricate glass/ceramic scaffolds. Fused deposition modeling of latticework scaffolds and extrusion of hydroxyapatite on the scaffolds was done by Cristina *et al*. [29] to fabricate scaffolds with high density. Simpson *et al*. [30] and Krishna *et al*. [31] studied the effect of pore sizes and pore geometry on mechanical and biological properties of scaffolds manufactured by selective laser sintering. 3D printing was also used to fabricate cell-laden poly (ε-caprolactone)/alginate hybrid scaffolds that showed over 83% cell proliferation and uniform distribution [32]. Foam replication technique was used by Chen *et al*. [33] to fabricate highly porous (90%) bioactive glass scaffolds. But most of the scaffolds fabricated using additive manufacturing techniques had low toughness compared to conventional methods like hot pressing.

This study aims at fabricating titanium reinforced glass scaffolds using freeform extrusion on to a hot plate. An aqueous paste mix of 13-39 silicate bioactive glass, binders and titanium fibers were made for extrusion. Four types of scaffolds, each having different quantities of titanium fibers (0, 0.2, 0.3 and 0.4 vol. %) were fabricated and their heat treatment schedule was identified. Following this a comprehensive evaluation of its

mechanical and biological properties was done. The mechanical properties tested include fracture toughness, flexural strength and compressive strength. In addition to this, bioactivity and degradation of mechanical strength *in vitro* were also assessed.

2. EXPERIMENTAL PROCEDURE

2.1. FABRICATION EQUIPMENT

A 3D printer that extrudes material onto a hot plate (Figure 2.1) is used for the fabrication of scaffolds. It primarily consists of extrusion devices, a motion subsystem and a real time control sub-system. The printer has X, Y and Z-axis motion capabilities controlled by three stepper motors (Empire Magnetics, Rohnert Park, CA). A ram extruder is used to provide the extrusion force.

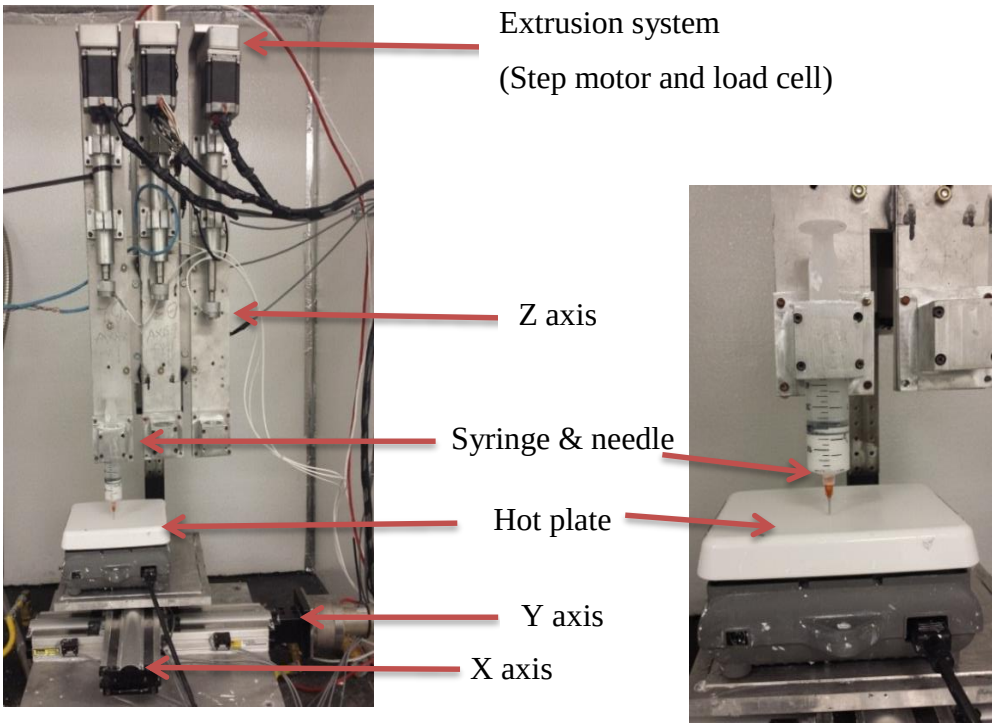

Figure 2.1. Overview of the machine used in the fabrication process

The paste in the syringe (60 cc plastic syringe) is extruded through a 1.19 mm nozzle (Nordson EFD, Westlake, OH) on to a hot plate set at 40 °C as shown in Figure 2.1.

After the completion of one layer, the gantry moves up by the thickness of one layer. These steps are repeated until the entire part is formed. For printing a scaffold, the scaffold geometry was modeled in NX 9.0 (CAD software from Siemens, Inc.) with the desired dimensions (40 x 36 x 6 mm^3), raster patterns, and pore size (800 μm) and later exported to the printer as G codes.

2.2. PREPARATION OF PASTE

The as-received water quenched 13-93 bioactive glass (50-56% silica, 17-23% calcium oxide, 3-5% phosphorous pentoxide, 5-7% sodium oxide, 10-14% potassium oxide, and 4-6% magnesium oxide, where the chemical composition is in weight.%) was crushed in a steel shatterbox (SPEX SamplePrep Crusher, Model 8500, Metuchen, NJ) and attrition-milled using de-ionized water for 3 h with ZrO_2 as the grinding medium. The particles' size distribution was measured using a laser diffraction-based particle size analyzer (Model LS 13 320; Beckman Coulter Inc., Fullerton, CA). To make an extrudable paste, the milled 13-93 bioactive glass particles were mixed with de-ionized water and additives including binder and dispersant. The mixture was then ball-milled for 18h with zirconium (grinding medium). Following milling, the mixture was heated for about 50 min at 70°C with continuous stirring along with the simultaneous addition of a thickening agent (Methocel) into the paste mix. Different types of pastes were used in this research with varying volume concentrations of titanium fibers (0.0, 0.2, 0.3 and 0.4 vol. %). For preparing a paste with fibers, the fibers were added to the stirring mix along with methocel. This ensured uniform distribution of fibers within the paste. Following this the paste was vacuum-mixed for 4-5 min (WhipMix Vacuum Power Mixer Plus; WhipMix Corporation,

Louisville, KY) so as to remove any air bubbles present and then transferred into an air-tight container. Figure 2.2 shows a paste with 0.3 vol. % of titanium fibers distributed in it. Since the fibers are added during the preparation of paste itself, a homogenous distribution is attained. The paste composition used is given in Table 2.1.

Figure 2.2. Paste with titanium fibers distributed in bioglass

Table 2.1. Titanium reinforced 13-39 bioactive glass paste composition

Component	Concentration (vol. %)	Manufacturer
13-93 Glass particles	40	Mo-Sci Corp, Rolla, MO
Darvan C	2	Vanderbilt Minerals LLC, Norwalk, CT
Methocel	4.0 – 4.4	Dow Chemical Company, Midland, MI
Titanium fiber	0.0 - 0.4	Intramicron LLC, Auburn, AL
De-ionized water	54	-

2.3. MATERIAL CHARACTERIZATION

The surface morphology of the scaffold was observed under a scanning electron microscope (S-4700; Hitachi, Tokyo, Japan) after coating it with Au/Pd. To analyze the presence of any crystalline phases in the as-received glass particles or in the sintered scaffold, X-ray diffraction (Philips X-Pert, Westborough, MA) was used. XRD was also used to check for the presence of hydroxyapatite on the surface of the scaffold, immersed in simulated body fluid (SBF). The surface of titanium fiber was examined for presence of oxides and carbides using an X-ray photoelectron spectrometer (Kratos Axis 165 Photoelectron Spectrometer, Manchester, UK).

2.4. POST PROCESSING

Thermogravimetric analysis (TGA) **(**NETZSCH STA 409 simultaneous thermal analyzer, Burlington, MA**)** was done on the green parts made with and without titanium fiber in order to identify the post processing schedule. The rate of heating, temperature holds, and sintering temperature were determined from the TGA results. Scanning electron microscopy (Hitachi S-4700 FESEM, Hitachi Co., Tokyo, Japan) images of green and sintered scaffolds were taken during most of the manufacturing and testing phases to look for visual clues towards defects in the scaffolds. X-ray diffraction (Philips X-Pert, Westborough, MA) run over 2θ range of 10° – 90° was used to identify the amorphous nature of sintered glass, as well as presence of titanium using Cu Kα radiation (λ = 0.154056 nm).

2.5. MECHANICAL PROPERTIES

2.5.1. Flexure Test. Scaffolds (3 x 5 x 25 mm^3) with different volume fraction of titanium fibers were tested in flexure using an Instron testing machine (model 5881, Norwood, MA). Prior to testing, surface grinding (FSG-618, Chevalier Machinery Inc., Santa Fe Springs, CA) was done to prepare parallel contact surfaces. A four point semi-articulated fixture (outer span of 20 mm and inner span of 10 mm) at a cross head speed of 0.2 mm/min using a 2 kN load cell was used in the flexure test and the load was applied along the z direction. The flexural stress was determined using the following equation (based on ASTM C1674-11):

$$\sigma = \frac{3Pl}{4bd^2}$$

where P is the applied force, l is the length of the outer span, b is the width and d is the thickness of the sample. The strength of the samples tested is expressed as mean ± standard deviation (SD).

2.5.2 Fracture Toughness Test. A chevron notched beam test was used to assess the fracture toughness of the scaffolds (3 x 5 x 25 mm^3). A notch was made at the mid span of the scaffold using a dicing saw (Accu-Cut 5200, AREMCO Products Inc., Ossining, NY) with a 0.15 mm thick diamond blade. A four-point, semi-articulated fixture mentioned above was used for this testing too. The fracture toughness was calculated using the following equation (based on ASTM C1421-10):

$$K_c = F_m Y^*_{min}(S_o - S_i)10^{-6}/BW^{3/2}$$

where K_c is the fracture toughness, F_m is the maximum load, S_o and S_i are outer and inner spans of the fixture used, B is the depth, and W is the width of the specimen. Y^*_{min} is the minimum of the geometric function (calculated based on ASTM C1421-10 guidelines). At least six samples each were tested for different levels of fiber. The toughness is expressed as mean ± standard deviation (SD).

2.6. *IN VITRO* ASSESSMENT OF SCAFFOLDS

For *in vitro* assessment two different scaffolds were used, one without fiber and one with 0.3 vol. % fiber. As-fabricated scaffolds (5 x 5 x 5 mm^3) were cleaned thrice in distilled water and then by ethanol using an ultrasonic cleaner (Crest CP 500T, Trenton, NJ), and dried overnight at 65 ℃ . The scaffolds were then weighed and immersed in simulated body fluid (SBF) prepared according to the Kokubo method with a starting pH of 7.40. 100 ml of SBF solution was used per gram of the scaffold, and the scaffold and SBF solution were placed in plastic Nalgene bottles. The samples were then kept in an incubator maintained at 37℃. Scaffolds were removed every week until four weeks, and then dried overnight. The following assessments were then performed.

2.6.1. Degradation of Compressive Strength in SBF. The scaffolds removed from SBF were tested in compression using an Instron testing machine (model 5881, Norwood, MA) at a crosshead speed of 0.5 mm/min using a 10 kN load cell. As mentioned, prior to testing the scaffolds were dried at 65℃ overnight. The compressive strength was

calculated by dividing the force by cross-sectional area. Five samples were used for compressive strength assessment and the strength is reported as mean ± SD.

2.6.2. Weight Loss of Scaffolds in SBF. Weight of the scaffolds were measured before immersing in SBF solution. After removal the weight was measured only after drying them overnight at 65℃. The weight loss was calculated according to the following formula.

$$Weight\ Loss = \frac{W_b - W_a}{W_b} \times 100$$

where W_b is the initial dry weight of the sample and W_a is the dry weight of the sample after removal from SBF. The weight loss percentage is plotted against immersion time as to investigate physical and chemical changes to the scaffolds.

2.6.3. Quantification of Titanium Ion Release to SBF Solution. Inductively coupled plasma mass spectrometry (ICP-MS) was used to quantify the amount of any titanium related compounds/ions released from scaffolds to the SBF solution. A NexION 350D ICP-MS (PerkinElmer, Waltham, MA) instrument was used for conducting the study. This test can detect traces of elements to parts per billion levels. The estimated Ti instrument detection limit is 0.25 µg/L, instrument quantification limit is 0.5 µg/L, and quantification method detection limit (MDL) is 2.5 µg/L. The operating conditions used are listed in Table 2.2.

Table 2.2: Operating conditions for the ICP-MS test

ICP-MS Operating Condition	
Nebulizer Gas Flow (L/min)	1.04*
Auxiliary Gas Flow (L/min)	1.2
Plasma Gas Flow (L/min)	18
ICP RF Power (W)	1600
Analog Stage Voltage (V)	-1675
Pulse Stage Voltage (V)	1400
Cell Entrance Voltage (V)	-2
Cell Exit Voltage (V)	-2
Cell Rod Offset	-15
Sampler Cones	Platinum
Skimmer Cones	Platinum
Sample Introduction System	Cyclonic Spray Chamber with Meinhard Nebulizer
Analyte	Ti-47, Ti-49
Dwell Time (ms)	50

*Optimized daily

3. RESULTS AND DISCUSSION

3.1. FABRICATION OF SCAFFOLDS

The size distribution of attrition-milled glass particles is shown in Figure 3.1.a. The particles size varied from ~0.2 to ~12 µm with an average of 2.3 µm. The SEM images of the as-received and attrition-milled bioglass are given in Figure 3.1.b and 3.1.c respectively. A typical irregular shape of the milled glass particles can be observed which will aid in achieving appropriate viscous flow characteristics during sintering. The irregular shape combined with small particle size could potentially reduce the micro pores in the scaffolds.

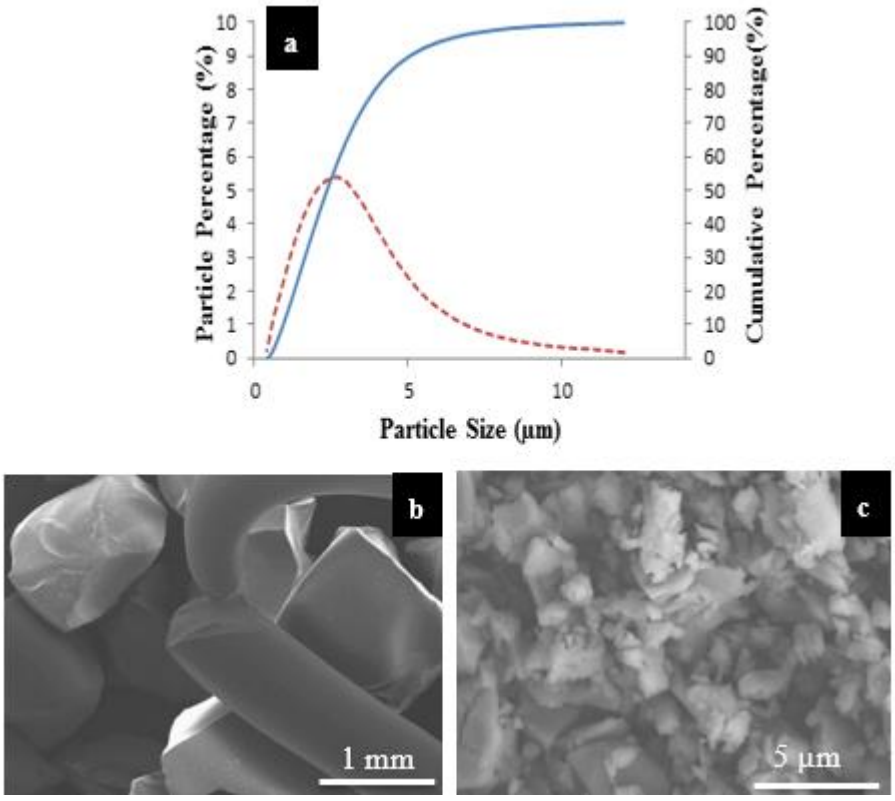

Figure 3.1. (a) Particle size distribution of attrition-milled bioglass (b) SEM image of the as-received glass particles (c) SEM image of attrition-milled glass particles.

The fabrication process consists of three basic steps: preparing the paste, printing the scaffolds, and sintering them. The attrition-milled bioglass was mixed with the additives listed in Table 2.1 to create a paste. The amount of titanium added to this paste varied based on the desired volume fraction. The paste making process is explained in detail in the appendix.

Scaffolds were fabricated using the extrusion fabrication machine (Figure 2.1). The prepared paste is filled into a syringe manually and is extruded onto a hot plate maintained at 40℃ using layer by layer deposition through a 1.19 mm diameter nozzle (Nordson EFD, Ohio, USA). The extrusion force used varied between 200 N and 320 N based on the amount of titanium fibers in the paste and the viscosity of the paste. An as-fabricated scaffold with a 0.3% volume fraction of fibers in it is depicted in Figure 3.2. The green scaffold was 40 mm x 36 mm x 6.0 mm in size and the pore sizes varied from 750 to 1000 μm.

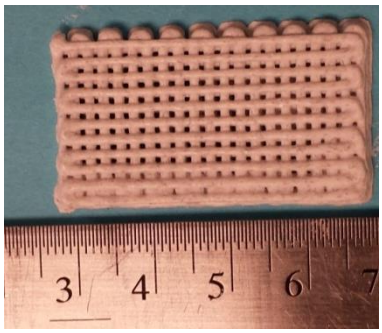

Figure 3.2. An as-fabricated scaffold with 0.3 vol. % titanium fiber.

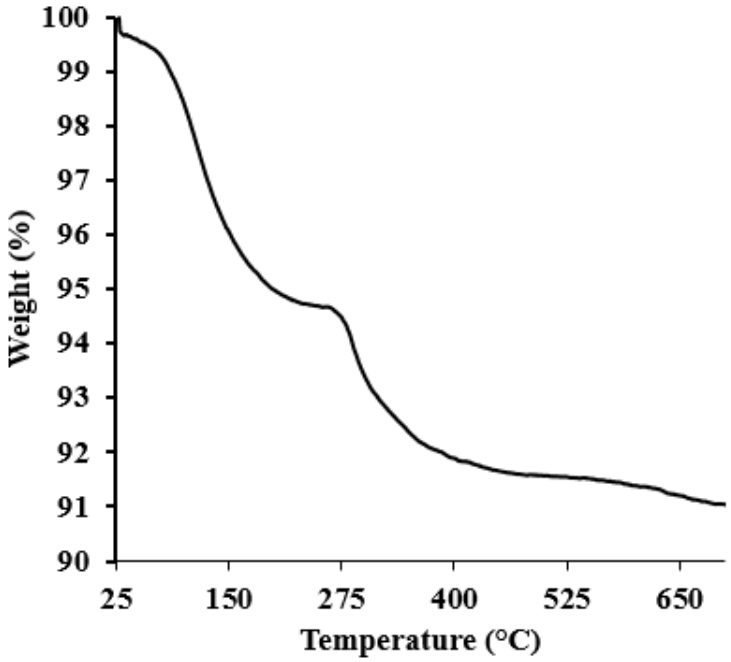

Figure 3.3. Thermogravimetric analysis of paste

The binder burnout schedule for the 'green scaffold' was developed from the thermogravimetric curve in Figure 3.3. This curve shows the changes in weight of the 'green scaffold' as a function of increasing temperature. Noticeable changes in the weight of the scaffold were observed at approximately 100 °C and 300 ℃. The residual water evaporates at 80-120 ℃ and Methocel and Darvan C burn out at around 300-350 ℃. Holding temperatures were designed based on the curve, as to aid slow burn-out of the additives in the scaffold. These observations were used to prepare the binder burnout and sintering schedule in Table 3.1.

Table 3.1. Binder Burnout Schedule

Starting Temperature (°C)	Ending Temperature (°C)	Heating Rate (°C/min)	Hold Period (h)
20	350	0.3	2
350	700	2	1
700	50	10	-

A sintered scaffold with 0.4 vol. % fiber is pictured in Figure 3.4.a. Shrinkage was observed in the final sintered part. The average shrinkage in the scaffold length, width and thickness was 25%, 29% and 17%, respectively. The pore sizes varied from 600 – 850 µm. Optical images (Figure 3.4.b, c) of the sintered scaffolds (shown in Figure 3.4.a) reveal that the fibers are dispersed in the glass matrix. Figure 3.c shows the sintered part a higher magnification. The Ti fibers oriented along the direction of the extruded filament can also be clearly observed in Figure 3.4.c.

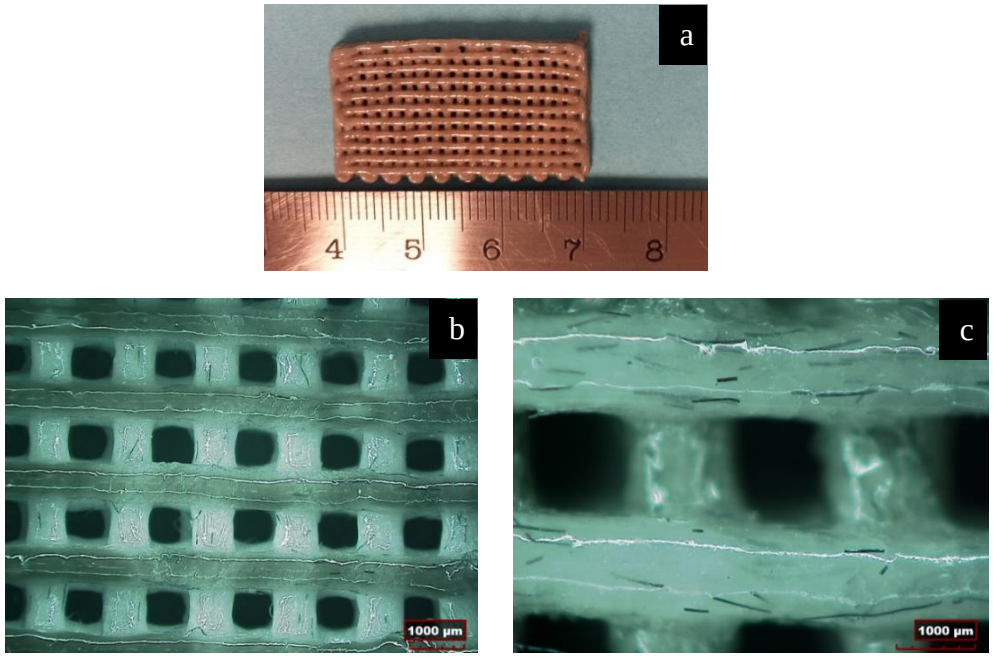

Figure 3.4. (a) Sintered 13-93 glass scaffold with 0.4 vol. % titanium fibers and (b) (c) Optical images of the corresponding scaffolds

XRD was conducted to verify that the sintered glass scaffold had an amorphous structure. The XRD patterns of both the sintered scaffold and the starting glass particles were found to have similar 'bumps' characteristic of amorphous materials under XRD (Figure 3.5). In an amorphous phase, i.e., when the atoms are randomly organized in the 3D space, X-rays will be scattered in many directions. This leads to large bumps along the 2Θ angle in the XRD patterns. These patterns made it clear that no considerable amount of crystallization was present in the final sintered scaffolds. XRD was also done on scaffolds that had different volume fractions of titanium fibers. All of the patterns revealed the amorphous nature of the final part. The XRD patterns of the scaffolds that had 0.4 vol. % fibers and as-received titanium fibers are given in Figure 3.6. The matching titanium fiber peaks (marked by red stars) in the scaffold with 0.4 vol% fiber can be seen in the XRD pattern.

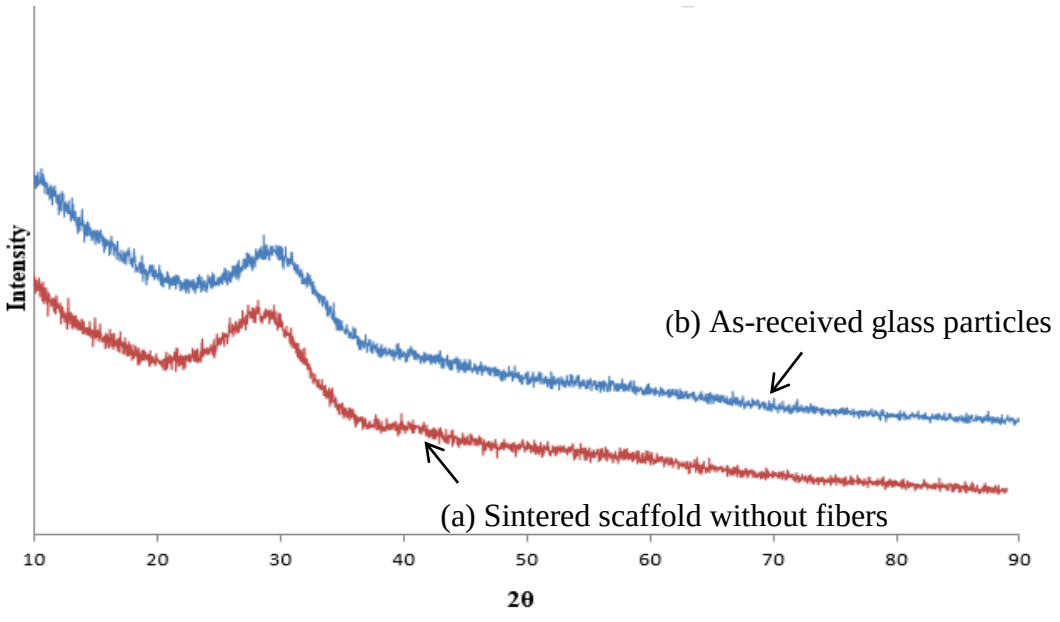

Figure 3.5. The XRD patterns of (a) a sintered scaffold without fibers and (b) a scaffold with as-received glass particles.

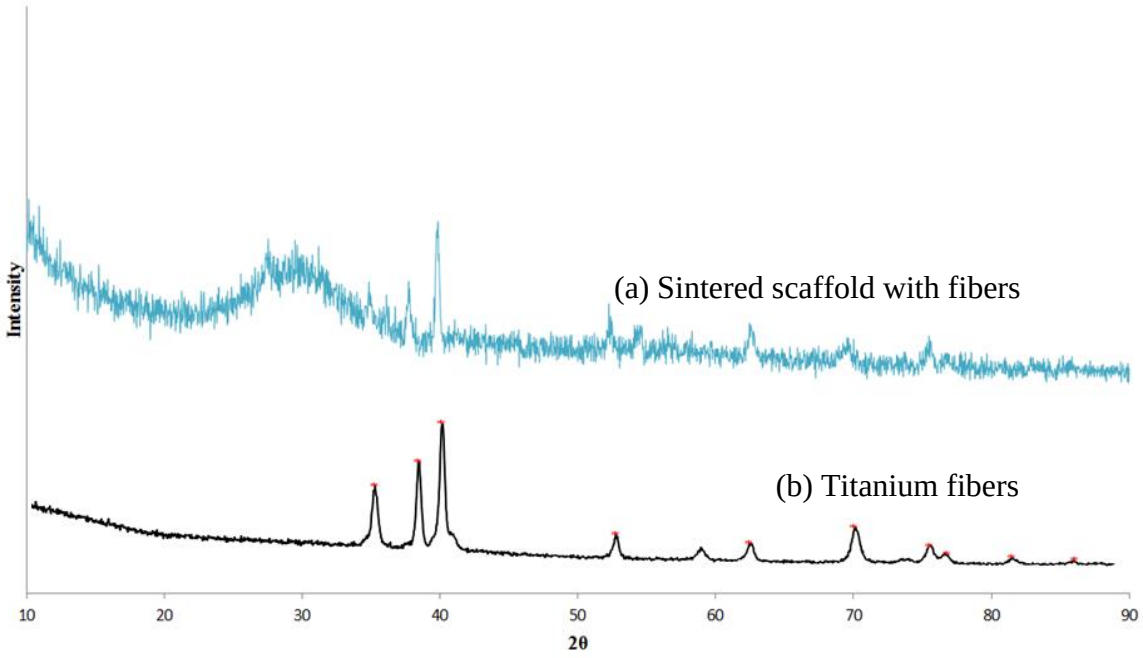

Figure 3.6. The XRD patterns of (a) a sintered scaffold with fibers and (b) the as received titanium fibers.

The titanium fibers had an average diameter of 16 μm and aspect ratio of 250. Their surface chemistry and morphology were each studied so as to better understand the fiber's bonding properties with the glass matrix. The SEM images of the fibers at varying magnifications are given in Figure 3.7. The fiber has uneven surface with irregularities that will help the glass matrix to better bond to the fiber and will aid in avoiding possible de-bonding during sintering process.

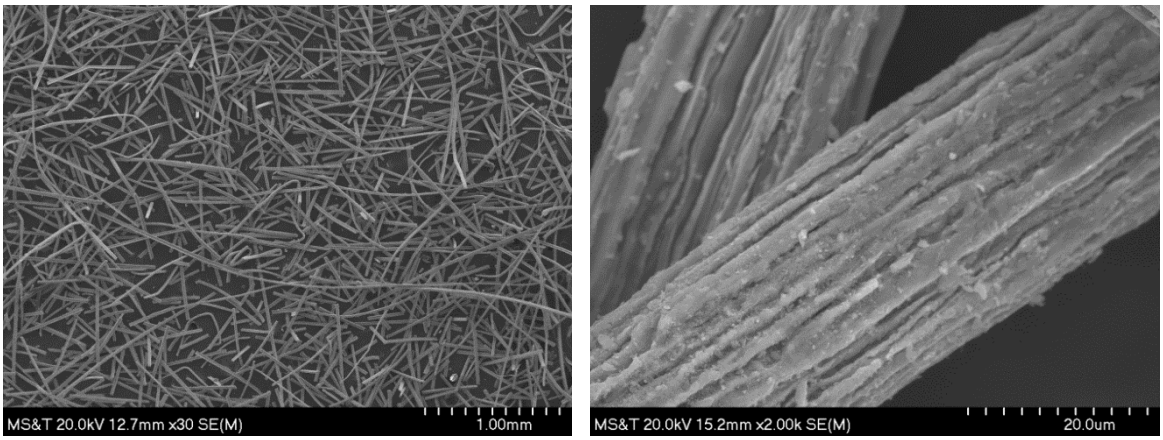

Figure 3.7 SEM images of fibers that reveal their rough surface.

XPS analysis was conducted on the fiber surface to analyze the surface chemistry of the fibers. In XPS analysis, X-rays are used to irradiate the surface of a material. The X-rays excite the electrons of the atoms on the surface of the material. If the X-ray energy is higher than the binding energy, electrons will be emitted from the surface. The kinetic energy of the emitted electrons is measured and subtracted from the incident energy of the X-ray to obtain the binding energy of that electron. From this, the element of atom can be determined. Further based on what element the parent atom is bonded to, the binding energy of the emitted electrons will vary. The instrument is capable of measuring such energy shifts. From this data, the chemical composition of any compound present of the surface could be determined. So essentially XPS result is a series of intensity peaks corresponding to binding energies of the photoelectrons emitted from the surface of the material. XPS can typically analyze the extreme outer thin layer (10-100 Angstroms) of a material. Figure 3.8 shows the pattern obtained after performing XPS analysis on the surface of the titanium fibers. The peaks for oxygen, titanium and carbon can be seen clearly from the pattern. Figure 3.9 shows the XPS pattern of the Ti-2p3 region from the

XPS pattern obtained. The peak for Ti 2p3 electron has convoluted peaks. The 2p3 binding energy values of these peaks are 457.60 eV, 459.2 eV and 462.8 eV. CasaXPS software was used to study the curve. These binding energy values correspond to titanium oxide, elemental titanium, and titanium carbide respectively. The presence of titanium oxides and carbides could result in slight changes in the thermal expansion coefficient of fibers. But after sintering, no observable de-bonding of fibers was observed.

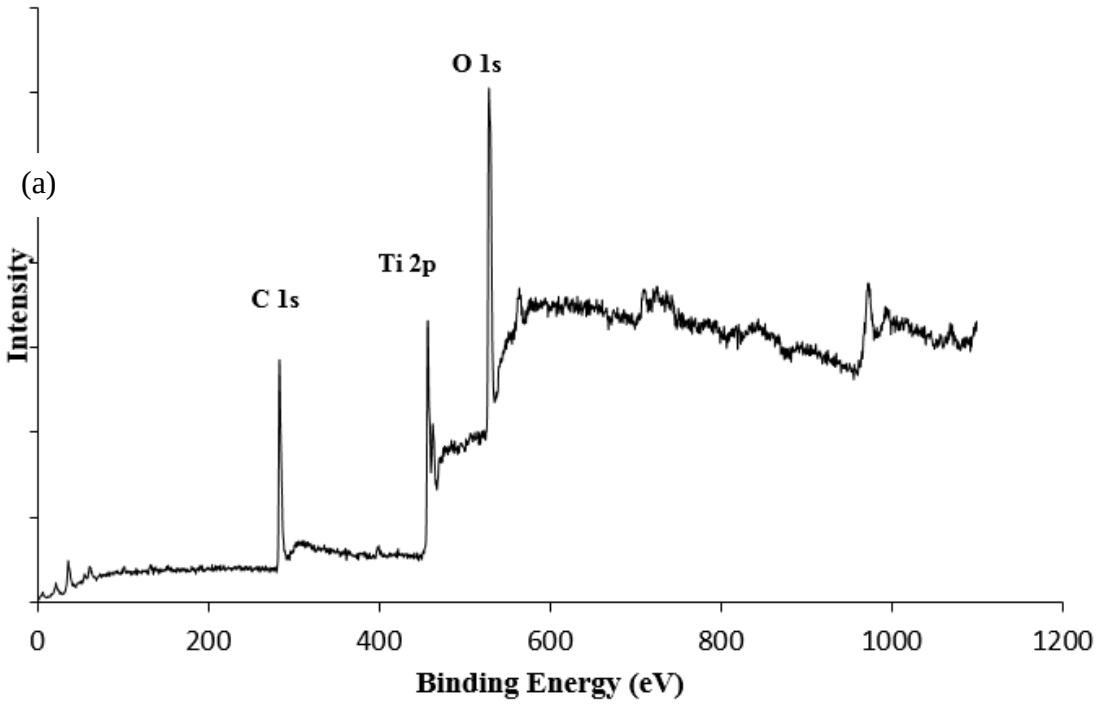

Figure 3.8. XPS pattern of (a) titanium fiber surface.

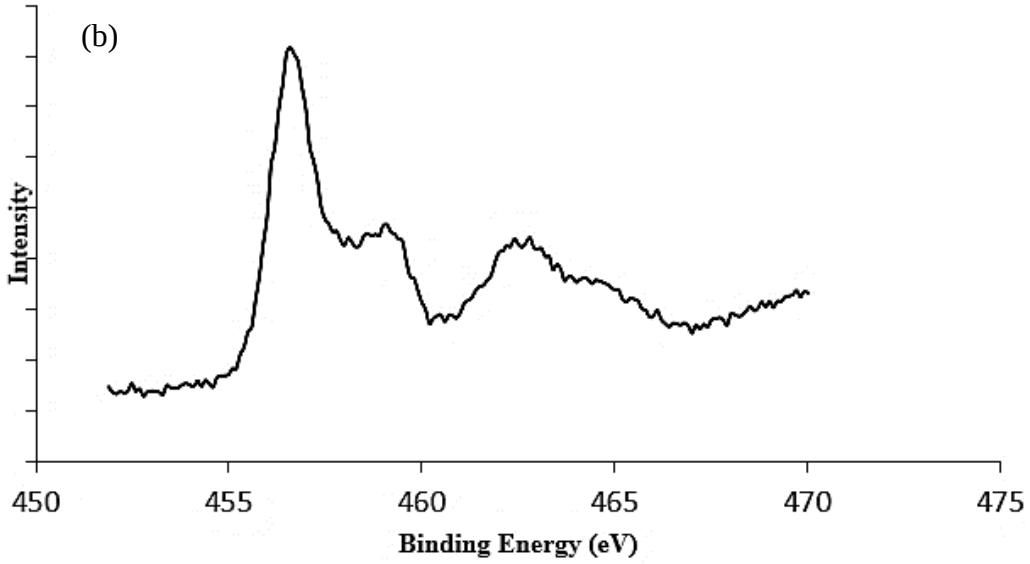

Figure 3.9. Detailed XPS pattern for Ti-2p3 peak observed in Figure 3.8

3.2. MECHANICAL PROPERTIES OF SCAFFOLDS

The flexural strength of scaffolds with varying vol. % of titanium fibers are summarized in Table 3.2. This strength varied from 10.4 MPa (0 vol. % of titanium fibers) to 14.9 Mpa (0.4 vol. % of titanium fibers). The flexural strength increased as the Ti fiber volume fraction increased. Previous mechanical testing studies on 13-93 bioglass scaffolds prepared by robocasting studies have shown that the value of flexural strength of 13-93 bioactive glass is in the range of 11 ± 3 MPa [18]. These values are similar to those obtained in this study. The flexural strength and flexural modulus of scaffolds with varying vol. % of fibers is listed in Table 3.2. The flexural modulus of the scaffolds increased to 15 GPa from 11 GPa due to addition of 0.4 vol. % titanium fibers into the scaffold. The trend in modulus clearly shows that the flexural strength increases with addition of fibers. The flexural strength reported in this study is similar to that of human trabecular bone (10-20 MPa) [34, 35].

Table 3.2 Flexural strength and flexural modulus of scaffolds with varying vol. % of titanium fibers

Fiber Volume Fraction (Vol.%)	#	Flexural Strength (MPa)	Average	Standard Deviation	Flexural Modulus (GPa)	Average	Standard Deviation
0.0	1	11.45	10.4	2.4	10.24	11.2	2.1
	2	9.57			12.79		
	3	7.97			9.1		
	4	12.35			11.02		
	5	8.15			10.96		
	6	7.55			13.3		
	7	13.71			9.87		
	8	12.75			12.15		
0.2	1	10.84	10.9	1.8	7.1	11.4	4.3
	2	9.56			9.65		
	3	11.01			7.99		
	4	12.45			12.91		
	5	8.34			15.52		
	6	11.22			8.56		
	7	9.92			14.03		
	8	13.97			15.7		
0.3	1	15.77	13.4	1.9	13.65	13.8	3.2
	2	13.34			16.93		
	3	14.27			10.6		
	4	11.87			14.37		
	5	10.95			11.12		
	6	15.75			12.49		
	7	11.46			17		
	8	13.62			15.88		
0.4	1	14.94	14.9	1.3	13.29	15.2	4.1
	2	16.56			19.24		
	3	14.78			11.10		
	4	13.98			15.75		
	5	15.63			19.31		
	6	13.75			12.18		
	7	16.46			11.96		
	8	12.87			18.87		

The fracture toughness of scaffolds with varying vol. % of titanium fibers is summarized in Table 3.3. The scaffolds with a 0.4 vol. % of titanium fibers were found to have the highest fracture toughness (~0.8 MPa•$m^{1/2}$) and those without fibers had a toughness of ~0.5 MPa•$m^{1/2}$. This trend indicates that the fracture toughness increases in a manner similar to that observed in flexural strength when the amount of fibers in the scaffold increases. The fracture toughness of scaffolds with varying vol. % of fibers with their standard deviation is summarized in Table 3.3. The trend in increase of toughness combined with increase in flexural modulus clearly shows that the mechanical properties are increasing with addition of fibers in the scaffolds.

Table 3.3. Fracture toughness of scaffolds with varying vol. % of fibers

Fiber Volume Fraction (Vol. %)	#	Fracture Toughness (MPa.$m^{1/2}$)	Average	Standard Deviation
0.0	1	0.42	0.47	0.03
	2	0.48		
	3	0.50		
	4	0.46		
	5	0.44		
	6	0.50		
0.2	1	0.58	0.59	0.06
	2	0.55		
	3	0.61		
	4	0.70		
	5	0.56		
	6	0.52		
0.3	1	0.61	0.71	0.13
	2	0.65		
	3	0.77		
	4	0.48		
	5	0.90		
	6	0.77		
0.4	1	0.81	0.79	0.07
	2	0.73		
	3	0.89		
	4	0.71		
	5	0.85		
	6	0.76		

Studies have shown that the mechanical properties of borosilicate glass matrix improved (five-fold improvement in fracture toughness to 3.85 $MPa.m^{1/2}$) due to addition of Hastelloy X fibers (15 vol. %) in them [25]. XPS analysis performed on the fibers showed a presence of TiO_2 on the surface of the Ti fibers. The presence of a layer of TiO_2 could aid in bonding of the Ti fiber with the 13-93 bioglass matrix which predominantly consists of several oxides including SiO_2. In addition, the rough and uneven surface of Ti fiber assists the bioglass matrix to better bond with the Ti fibers. An increased adhesion between the glass matrix and the Ti fibers will increase the strength of scaffolds [37]. Below a fine layer of TiO_2 on surface of the fibers, pure elemental Ti is present at the core. The Ti fibers have an average tensile strength in the range from 246 to 370 MPa which would help reinforce the brittle glass matrix by transferring the bending stresses from the matrix to the fibers [36, 25].

In this study, titanium fibers were added during the production of paste and not during the fabrication process. This type of pre-impregnation creates a homogenous matrix, which in turn increases the strength considerably as compared to when the fibers are added manually. The thermal expansion coefficients of the 13-93 bioglass and the titanium fibers were 8.6×10^{-6} m/m K and 10.2×10^{-6} m/m K, respectively. After sintering, the glass matrix will be in contraction and the Ti fibers will be in tension, preserving the bond between the matrix and fiber. An enhanced matrix-fiber adhesion can modify the character of local stresses. It can also impact the connectivity of the yielded micro zones adjacent to neighboring fibers resulting in an increase of the mechanical properties of the scaffolds [38].

The addition of fibers improves the resistance of the scaffolds to crack propagation. There are basically three possibilities once the crack reaches a fiber: (i) The crack propagates through the fiber either by breaking the fiber or by plastic deformation; (ii) deflection of the crack due to the fiber, and along a weaker fiber-matrix interface; and (iii) a localized de-bonding occurs at the fiber-glass interface and the crack propagation energy is dissipated, resulting in delayed/no crack propagation.

As to better understand crack propagation, pressed pellets (with bioactive glass and fibers) were fabricated. On the pellets, indents were made using a Vickers indenter (Struers Duramin-500, Cleveland, OH) and the propagation of cracks was studied using an optical microscope. Figure 3.10 reveals that the fiber delays the growth of crack through it. In addition Figure 3.10 shows a crack deflecting along the fiber-matrix interface and finally propagating through it. This kind of 'deflections' are also effective toughening mechanisms as they delay the crack propagation. The arrows in the Figure 3.10 shows the deflections in crack near the fiber.

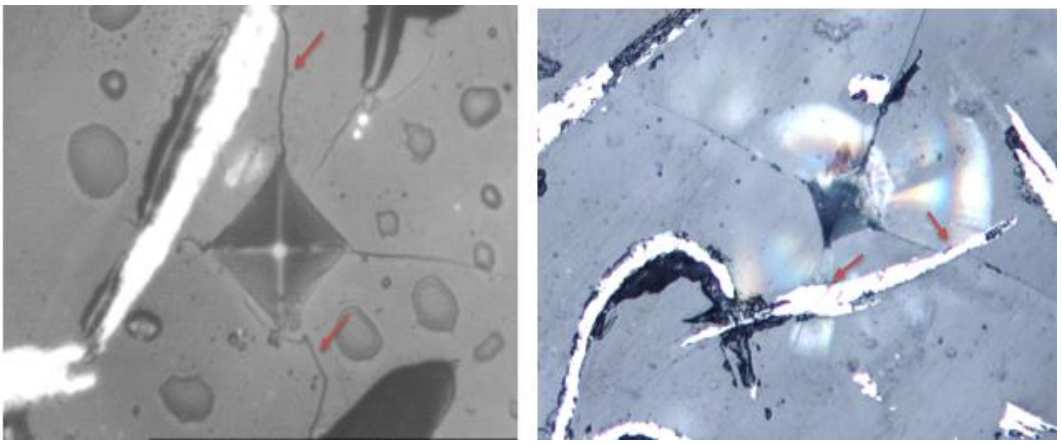

Figure 3.10. Crack deflections resulting in delay of crack growth through the glass matrix

3.3. IN-VITRO EVALUATION OF SCAFFOLDS

Degradation of compressive strength of scaffolds, both with and without fibers as a function of immersion time in SBF can be seen in Figure 3.11. The compressive strength of scaffolds without fibers, before immersion, was 103 ± 33 MPa. This strength was reduced to 67 MPa (reduction by ~30 %) after the scaffolds were immersed in SBF for four weeks. This reduction is in accordance with similar studies conducted previously [17]. The scaffold's strength with fibers, before immersion, was 128 ± 30 MPa. This strength was reduced by ~39% after 4 weeks to 88 MPa. The compressive strengths obtained (before immersion into SBF) are similar to that of human cortical bone [34, 35]. The scaffolds lost weight when hydroxyapatite was formed on the surface and elements dissociated into the SBF solution. The weight loss of scaffolds, both with and without fibers as a function of immersion time is given in Figure 3.12. The weight loss in the first two weeks was ~ 8%, because of hydroxyapatite formed on the fresh surface. The weight loss decreased in the third and fourth week (~ 3%). This trend is similar to that observed in compressive strength. This weight loss could also be a potential reason behind the reduction in compressive strength *in-vitro*.

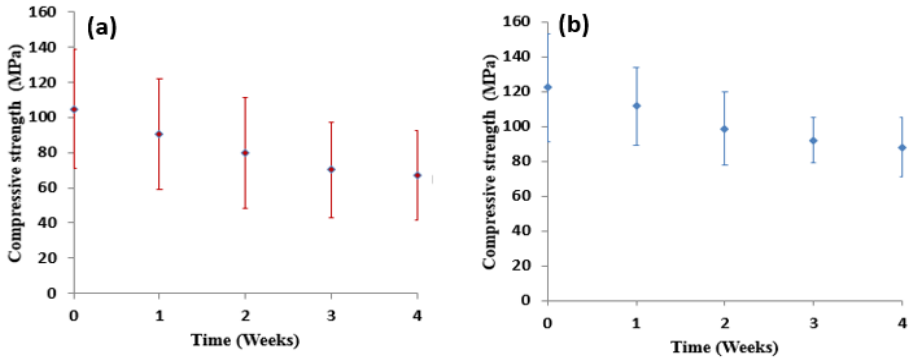

Figure 3.11. Variation in the compressive strength of: (a) scaffolds without fibers; (b) with fibers, when immersed in SBF.

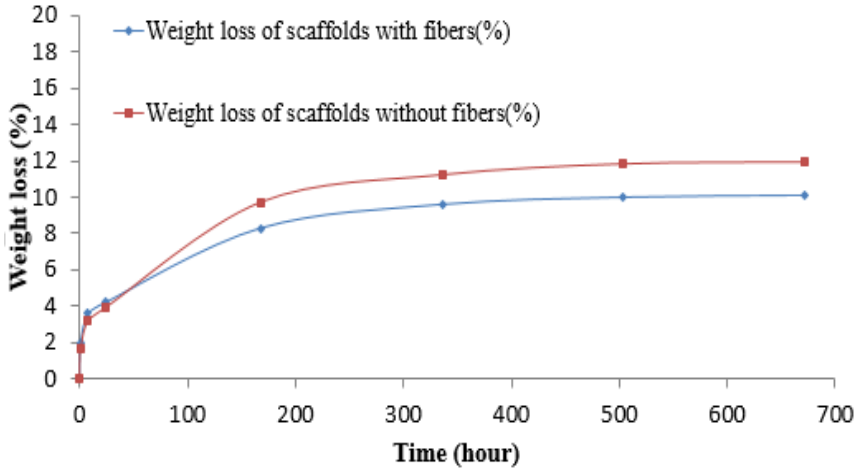

Figure 3.12. Weight loss of scaffolds with and without fiber in SBF as a function of time.

The SEM images of a scaffold surface, with fibers immersed in SBF for two weeks are given in Figure 3.13. A thick crystalline layer with cracks was formed on the surface. Needle-like structures similar to that of hydroxyapatite were observed at a higher magnification [13, 18, 23]. A fiber that pulled out of the glass matrix can be seen in Figure 3.13.c. Since the fiber was pulled out from the bioglass matrix, it had a bioglass residuals on the surface. A hydroxyapatite like material can be seen at the tip of this fiber, mostly due to conversion of bioglass residuals on the surface of the fiber. The XRD pattern that was received after the scaffolds (both with and without fibers) were analyzed, had peaks that matched to the reference synthetic HA (JCPDS 72-1243), as pictured in Figure 3.14. The patterns for scaffolds with and without fibers were identical, likely because of the low volume fraction of Ti fibers used.

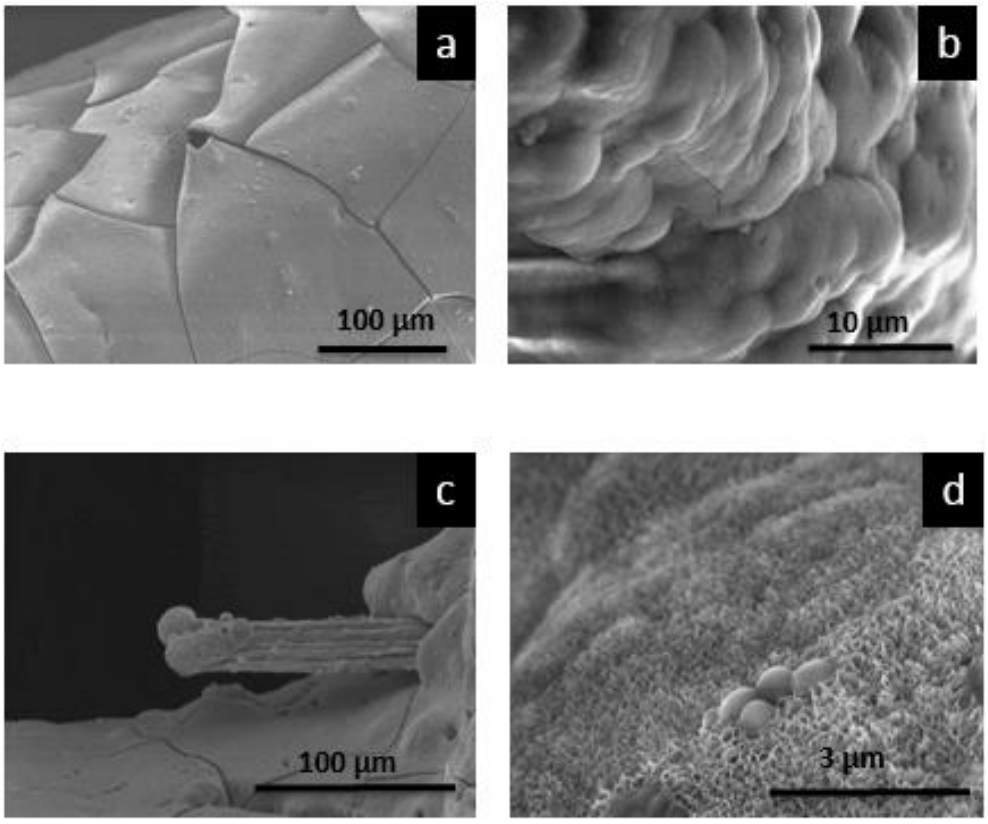

Figure 3.13. SEM images of (a) Surface of scaffolds after immersion in SBF for 2 weeks at 1000X, (b) magnified image of the same surface at 10000X , (c) fiber on the surface of the scaffold at 1000X, (d) needle like HA crystals formed on the surface at 33000X.

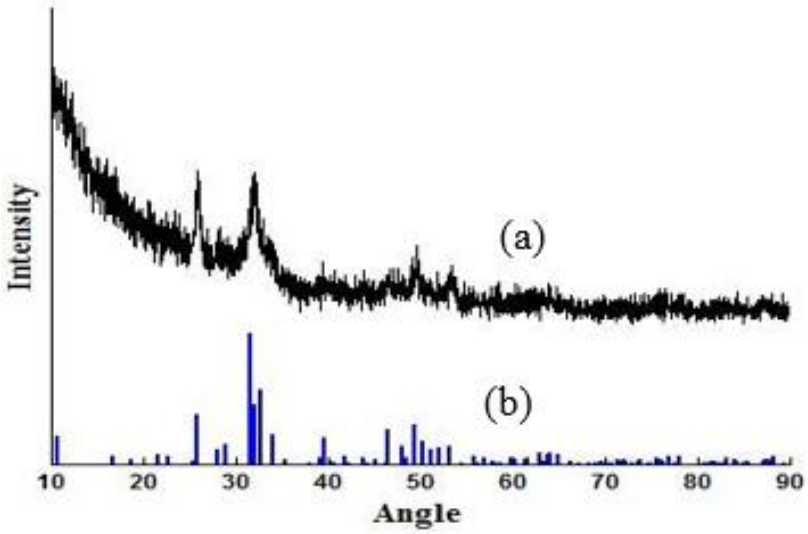

Figure 3.14. The XRD patterns of (a) the scaffold with 0.3 vol. % of fibers immersed in SBF for 2 weeks and (b) the reference hydroxyapatite (JCPDS 72-1243).

The results gathered from the ICP-MS test are listed in Table 3.4. The concentration of Ti in SBF solution after four weeks of immersion was 0.26 µg/L. It can be seen that at the end of 2 weeks, the Ti concentration was 0.32 µg/L. The concentrations listed are for a total of five scaffolds immersed in SBF. The titanium fibers on the surface of the scaffold's surface came into contact with the SBF solution during the initial four weeks. In case of scaffolds immersed in SBF for both three and four weeks, the amount of fibers on the surface that was exposed to SBF solution was low. This is the primary reason behind low titanium ion concentration rates as compared to the scaffolds that were used in the first two weeks.

Table 3.4 Titanium ion concentration in SBF solution

Sample		**Titanium concentration (µg/L)**
Quality control blank		<< 0.25
Scaffolds with	1 week	0.30
	2 weeks	0.32
	3 weeks	0.25
	4 weeks	0.26

The formation of hydroxyapatite confirms the bioactivity of the scaffolds. When the bioglass scaffolds are placed in the SBF solution Na^+, K^+ and $(SiO_4)^{4-}$ ions dissolve into the solution. Hydroxyapatite is formed due to the reaction of CaO present in the bioglass with phosphate ions in the SBF solution. In conversion of silicate based 13-93 bioglass, a thin layer of SiO_2 is formed on the surface of scaffolds on exposure to SBF solution. This primarily slows down the conversion rate after a few days as shown by the weight loss data. Since the volume fraction of fibers added was low (0.3 vol.%), a considerable difference in weight loss due to addition of fibers was not observed.

The conversion of bioglass scaffolds into hydroxyapatite also results in the reduction of its mechanical properties. This is shown by the reduction in the compressive strength of the scaffolds (Figure 3.12). The reduction in the compressive strength of both types of scaffolds, with and without fibers, is a desirable property of bone implants. The scaffolds with fibers had average compressive strength of 88 MPa after being immersed in the SBF solution for four weeks. The high strength (88 MPa) of the scaffolds, even after immersion in SBF for four weeks, leads to the possibility that the scaffolds could be used for load bearing applications.

A significant amount of titanium ions remained absent from the SBF solution even after four weeks of immersion of the scaffolds (titanium ions in the solution for five scaffolds was < 0.4 µg/L). Previous studies on Ti implants have shown that Ti surface on exposure to body fluids (20 mL Hank's solution of pH 4.0) , develops a thin coating of titanium dioxide on its surface [39]. This provide high corrosion resistance and biocompatibility to the titanium implant. Joesph *et al.* [40], studied the release of Ti ions from titanium and $TiAl_6Nb_7$ samples (10 mm x 10 mm x 1 mm) in different body fluids (20 mL Hank's solution of pH 4.0) for an extended period of 12 weeks. The concentration of Ti ions reported after 12 weeks was 0.6 mg/L. Fabian *et al.* [41] investigated the effect of TiO_2 nano particles injected intravenously into rat body on the normal functionality. 5 mg/kg of TiO_2 was the dose used in this study. However no toxic effect was evident from the experimental results. The study concluded that TiO_2 at low concentration (< 5 mg/kg) is not toxic and can be used safely in implants. Frisken *et al.* [42], studied the titanium release into body organs after insertion of a screw implant into the mandibles of a sheep

for 12 weeks. According to that study, minor elevations in Ti levels (300 ppb of Ti) were observed in the lungs and lymph nodes. But the concentration is unlikely to cause a health problem. The study, however, warns using multiple implants, as the amount of Ti released will be comparatively high as to cause a significant level of toxicity. The titanium ions released into SBF solution in our study is < 0.4 µg/L, when compared to the amounts mentioned above. The chances of a systemic effect due to the leaching out of titanium ions from the fibers in the scaffolds at the current concentration should be negligible. The fibers are likely to become embedded in the newly formed bone as the new bone grows through the scaffolds.

4. CONCLUSION

This study investigated the feasibility of fabricating titanium fiber reinforced 13-93 bioglass scaffolds using the freeform extrusion fabrication technique. Scaffolds reinforced with 0.4 vol. % fibers had a fracture toughness of ~ 0.8 MPa•$m^{1/2}$ and flexural strength of ~ 15 MPa. The fracture toughness of scaffolds with fibers increased by 70% compared to that without fibers and the flexural strength increased by 40%. The *in vitro* assessment of scaffolds revealed that the addition of biocompatible titanium fibers to the bioactive glass reinforced the scaffold mechanically without inhibiting its bioactive properties. The improved mechanical properties with compressive strengths of ~88 MPa even after four week degradation in simulated body fluid shows the potential of the 13-93 bioglass+Ti composite implants for load bearing bone repair applications.

APPENDIX

Recipe for preparing 13-93 bioactive glass paste

1. Fill a 500 ml Nalgene bottle one-third of the way with zirconia media.
2. Weight out 110 g of attrition milled 13-93 bioactive glass into it.
3. Add 54 ml of water along with 1.13 ml of Darvan C to the above mixture.
4. Close the bottle and shake it by hand for a couple of minutes as to prepare a slurry.
5. Ball mill for ~18 hours at 40 rpm.
6. After the ball milling operation, connect the water jacket to water bath. Place the beaker on top of a stir plate. Set the water bath to 70°C. Do not remove the bottle off the ball mill until the water reaches 70°C.
7. Once the set temperature is reached, put a stir bar in the beaker and set it to speed 400 RPM. Pour the slurry into the water jacketed beaker. Make sure the media do not fall into the beaker.
8. Cover the beaker with a watch glass.
9. While waiting for the water bath temperature to come back to 70°C, weigh out 3.5 g of Methocel.
10. Lifting the watch glass with one hand put a small amount of Methocel with a spatula in the other hand. Cover the beaker with the watch glass while the Methocel added is stirred into the slurry. Although the Methocel should be added slowly, the beaker should not remain uncovered for long since that will lead to water evaporation and the paste will not turn out as expected.
11. Once all the Methocel is added in, let the slurry stir for 5 minutes.

12. Now weigh out the required amount of fibers (based on the Vol % required) and add it slowly into the above mixture.
13. After 5 minutes, set the water bath to 20°C. Make sure to check on it every once in a while. If a layer starts forming, stir the slurry with the spatula. The paste will start setting. When the stir bar cannot possibly stir the paste, turn off the stir plate.
14. When the water bath reaches 20°C, use the spatula to put the paste in the Whip Mixer container. Close it with the lid. Connect the vacuum line. Turn it on. Whip mix it for 5 minutes. Using a cooking spatula, scrape the paste off the blade. Whip mix it another 5 minutes. Let it cool for 2 minutes. Whip mix it another 5 minutes for a total of 15 minutes.
15. Disconnect the vacuum line. Turn the Whip Mix on for a minute to clean the line and lubricate the motor.
16. Using a cooking spatula put the paste in a bottle.

BIBLIOGRAPHY

[1] Bates P, Ramachandran M. "Bone injury, healing and grafting. " In Basic Orthopaedic Sciences. The Stanmore Guide. Edited by Ramachandran M. London: Hodder Arnold; 2007:123-134.

[2] Einhorn, Thomas A. "The Cell And Molecular Biology Of Fracture Healing." Clinical Orthopaedics And Related Research, 1998, S7-S21.

[3] Gugala, Zbigniew, Ronald W. Lindsey, and Sylwester Gogolewski. "New Approaches in the Treatment of Critical-Size Segmental Defects in Long Bones." Macromolecular Symposia, 2007, 147-61.

[4] Dimitriou, Rozalia, Elena Jones, Dennis Mcgonagle, and Peter V Giannoudis. "Bone Regeneration: Current Concepts and Future Directions." BMC Medicine 9:66 (2011): 66.

[5] Lasprilla, A. J. R., G. A. R. Martinez, B. H. Lunelli, A. L. Jardini, and R. Maciel Filho. "Biomaterials for application in bone tissue engineering." *Journal of Biotechnology* 150 (2010): 455.

[6] Stevens, Molly M. "Biomaterials for bone tissue engineering." *Materials today* 11, no. 5 (2008): 18-25.

[7] Thoma, D. S., A. Kruse, C. Ghayor, R. E. Jung, and F. E. Weber. "Bone augmentation using a synthetic hydroxyapatite/silica oxide-based and a xenogenic hydroxyapatite-based bone substitute materials with and without recombinant human bone morphogenetic protein-2." *Clinical oral implants research* (2014)

[8] Yamamoto, Masaya, Akishige Hokugo, Yoshitake Takahashi, Takayoshi Nakano, Masahiro Hiraoka, and Yasuhiko Tabata. "Combination of BMP-2-releasing gelatin/β-TCP sponges with autologous bone marrow for bone regeneration of X-ray-irradiated rabbit ulnar defects." *Biomaterials* 56 (2015): 18-25.

[9] Johnson, Amy J. Wagoner, and Brad A. Herschler. "A review of the mechanical behavior of CaP and CaP/polymer composites for applications in bone replacement and repair." *Acta biomaterialia* 7, no. 1 (2011): 16-30.

[10] Hutmacher, Dietmar W., Thorsten Schantz, Iwan Zein, Kee Woei Ng, Swee Hin Teoh, and Kim Cheng Tan. "Mechanical properties and cell cultural response of polycaprolactone scaffolds designed and fabricated via fused deposition modeling." *Journal of biomedical materials research* 55, no. 2 (2001): 203-216.

[11] Shor, Lauren, Selçuk Güçeri, Xuejun Wen, Milind Gandhi, and Wei Sun. "Fabrication of three-dimensional polycaprolactone/hydroxyapatite tissue scaffolds and osteoblast-scaffold interactions in vitro." *Biomaterials* 28, no. 35 (2007): 5291-5297.

[12] Rahaman, Mohamed N., Roger F. Brown, B. Sonny Bal, and Delbert E. Day. "Bioactive glasses for nonbearing applications in total joint replacement." In *Seminars in Arthroplasty*, vol. 17, no. 3, pp. 102-112. WB Saunders, 2006.

[13] Fu, Qiang, Mohamed N. Rahaman, B. Sonny Bal, Wenhai Huang, and Delbert E. Day. "Preparation and bioactive characteristics of a porous 13–93 glass, and fabrication into the articulating surface of a proximal tibia." *Journal of Biomedical Materials Research Part A* 82, no. 1 (2007): 222-229.

[14] Liu, Xin, Mohamed N. Rahaman, Qiang Fu, and Antoni P. Tomsia. "Porous and strong bioactive glass (13-93) scaffolds prepared by unidirectional freezing of camphene-based suspensions." *Acta biomaterialia* 8, no. 1 (2012): 415-423.

[15] Kolan, Krishna CR, Ming C. Leu, Gregory E. Hilmas, Roger F. Brown, and Mariano Velez. "Fabrication of 13-93 bioactive glass scaffolds for bone tissue engineering using indirect selective laser sintering." *Biofabrication* 3, no. 2 (2011): 025004.

[16] Doiphode, Nikhil D., Tieshu Huang, Ming C. Leu, Mohamed N. Rahaman, and Delbert E. Day. "Freeze extrusion fabrication of 13–93 bioactive glass scaffolds for bone repair." *Journal of Materials Science: Materials in Medicine* 22, no. 3 (2011): 515-523

[17] Fu, Qiang, Mohamed N. Rahaman, B. Sonny Bal, and Roger F. Brown. "Preparation and in vitro evaluation of bioactive glass (13–93) scaffolds with oriented microstructures for repair and regeneration of load-bearing bones." *Journal of Biomedical Materials Research Part A* 93, no. 4 (2010): 1380-1390.

[18] Fu, Qiang, Mohamed N. Rahaman, B. Sonny Bal, Roger F. Brown, and Delbert E. Day. "Mechanical and in vitro performance of 13–93 bioactive glass scaffolds prepared by a polymer foam replication technique." *Acta Biomaterialia* 4, no. 6 (2008): 1854-1864.

[19] Liu, Xin, Mohamed N. Rahaman, Gregory E. Hilmas, and B. Sonny Bal. "Mechanical properties of bioactive glass (13-93) scaffolds fabricated by robotic deposition for structural bone repair." *Acta biomaterialia* 9, no. 6 (2013): 7025-7034.

[20] Liu, Xin, Mohamed N. Rahaman, Yongxing Liu, B. Sonny Bal, and Lynda F. Bonewald. "Enhanced bone regeneration in rat calvarial defects implanted with surface-modified and BMP-loaded bioactive glass (13-93) scaffolds." *Acta biomaterialia* 9, no. 7 (2013): 7506-7517

[21] Lin, Yinan, Wei Xiao, Xin Liu, B. Sonny Bal, Lynda F. Bonewald, and Mohamed N. Rahaman. "Long-term bone regeneration, mineralization and angiogenesis in rat calvarial defects implanted with strong porous bioactive glass (13–93) scaffolds." *Journal of Non-Crystalline Solids* (2015)

[22] Velez, M., S. Jung, K. C. R. Kolan, M. C. Leu, D. E. Day, and T-MG Chu. "In Vivo Evaluation of 13-93 Bioactive Glass Scaffolds Made by Selective Laser Sintering (SLS)." *Biomaterials Science: Processing, Properties and Applications II: Ceramic Transactions, Volume 237* (2012): 91-99.

[23] Kolan, Krishna CR, Ming C. Leu, Gregory E. Hilmas, and Mariano Velez. "Effect of material, process parameters, and simulated body fluids on mechanical properties of 13-93 bioactive glass porous constructs made by selective laser sintering." *Journal of the mechanical behavior of biomedical materials* 13 (2012): 14-24.

[24] Troczynski, Thomas B., Patrick S. Nicholson, and Carmen E. Rucker. "Inclusion-Size-Independent Strength of Glass/Particulate-Metal Composites." *Journal of the American Ceramic Society* 71, no. 5 (1988): C-276.

[25] Troczynski, Thomas B., and Patrick S. Nicholson. "Fracture Mechanics of Titanium/Bioactive Glass-Ceramic Particulate Composites." *Journal of the American Ceramic Society* 74, no. 8 (1991): 1803-1806.

[26] Blaker, J. J., S. N. Nazhat, and A. R. Boccaccini. "Development and characterisation of silver-doped bioactive glass-coated sutures for tissue engineering and wound healing applications." *Biomaterials* 25, no. 7 (2004): 1319-1329.

[27] Cesarano, Joseph, Jennifer G. Dellinger, Michael P. Saavedra, David D. Gill, Russell D. Jamison, Benjamin A. Grosser, Janet M. Sinn-Hanlon, and Michael S. Goldwasser. "Customization of Load-Bearing Hydroxyapatite Lattice Scaffolds." *International Journal of Applied Ceramic Technology* 2, no. 3 (2005): 212-220.

[28] Lorrison J C, Goodridge R D, Dalgarno K W and Wood D J. Selective laser sintering of bioactive glass-ceramicsProc. 13th Annual Int. Solid Freeform Fabrication Symp.(Austin, TX) (2002): 1–8.

[29] Sousa, F., and Julian RG Evans. "Sintered hydroxyapatite latticework for bone substitute." *Journal of the American Ceramic Society* 86, no. 3 (2003): 517-519.

[30] Simpson, Rebecca Louise, Florencia Edith Wiria, Andrew A. Amis, Chee Kai Chua, Kah Fai Leong, Ulrich N. Hansen, Margam Chandrasekaran, and Mun Wai Lee. "Development of a 95/5 poly (L-lactide-co-glycolide)/hydroxylapatite and β-tricalcium phosphate scaffold as bone replacement material via selective laser sintering." *Journal of Biomedical Materials Research Part B: Applied Biomaterials* 84, no. 1 (2008): 17-25.

[31] Kolan, Krishna CR, Albin Thomas, Ming C. Leu, and Greg Hilmas. "In vitro assessment of laser sintered bioactive glass scaffolds with different pore geometries." *Rapid Prototyping Journal* 21, no. 2 (2015): 152-158.

[32] Lee, HyeongJin, SeungHyun Ahn, Lawrence J. Bonassar, Wook Chun, and GeunHyung Kim. "Cell-laden poly (ε-caprolactone)/alginate hybrid scaffolds fabricated by an aerosol cross-linking process for obtaining homogeneous cell distribution: fabrication, seeding efficiency, and cell proliferation and distribution." *Tissue Engineering Part C: Methods* 19, no. 10 (2013): 784-793

[33] Chen, Qizhi Z., Ian D. Thompson, and Aldo R. Boccaccini. "45S5 Bioglass®-derived glass–ceramic scaffolds for bone tissue engineering." *Biomaterials* 27, no. 11 (2006): 2414-2425.

[34] M. Keaveny, W.C. Hayes, in: B.K. Hall (Ed.), Bone. A Treatise, CRC Press, Boca Raton, FL, 1993, pp. 285

[35] Fung, Yuan-Cheng. *Biomechanics: mechanical properties of living tissues*. Springer Science & Business Media, 2013.

[36] Donachie, Matthew J. *Titanium: a technical guide*. ASM international, 2000.

[37] Yeomans, J. A. "Ductile particle ceramic matrix composites—Scientific curiosities or engineering materials?." *Journal of the European Ceramic Society* 28, no. 7 (2008): 1543-1550.

[38] Claxton, E., B. A. Taylor, and R. D. Rawlings. "Processing and properties of a bioactive glass-ceramic reinforced with ductile silver particles." *Journal of materials science* 37, no. 17 (2002): 3725-3732

[39] Smith, G. K. "Systemic aspects of metallic implant degradation." *Biomaterials in reconstructive surgery. St. Louis: Mosby* (1983): 229.

[40] Joseph, Lori A., Omoniyi K. Israel, and Ekanem J. Edet. "Comparative evaluation of metal ions release from titanium and Ti-6Al-7Nb into bio-fluids." *Dental research journal* 6, no. 1 (2009): 7.

[41] Fabian, E., Landsiedel, R., Ma-Hock, L., Wiench, K., Wohlleben, W., & Van Ravenzwaay, B. (2008). Tissue distribution and toxicity of intravenously administered titanium dioxide nanoparticles in rats. *Archives of toxicology*, *82*(3), 151-157.

[42] Frisken, K. W., Dandie, G. W., Lugowski, S., & Jordan, G. (2002). A study of titanium release into body organs following the insertion of single threaded screw implants into the mandibles of sheep. *Australian dental journal*, *47*(3), 214-217.

VITA

Albin Thomas was born on November 24th, 1991 in Kerala, India. In May 2013 he received his Bachelor of Technology degree with honors in Mechanical Engineering from Guru Ghasidas Vishwavidyalaya, Bilaspur, India.

In August 2013 he joined Missouri University of Science and Technology to pursue his Master's degree in Mechanical Engineering. He was a graduate teaching and research assistant in addition to being a student technical assistant during his two years of studies at the master's level. In August 2015 he graduated with a Master of Science degree in Mechanical Engineering.